Supporting Material: The Larmor frequency shift of a white matter magnetic microstructure model with multiple sources

Here we present the derivation of the mesoscopic Larmor frequency shift $\overline{\Omega}(\mathbf{R})$, Equation (1), from our white matter magnetic microstructure model. This entails finding the total Lorentzian tensor $\mathbf{L}$, Equation (3), which consist of three main parts: (**A1**) the induced frequency shift in cylinders from cylinders, (**A2**) the induced frequency in spheres from the spheres, (**A3**) the induced frequency in either cylinders or spheres from the magnetized spheres or cylinders, respectively. All these contributions will be considered in turn.

Integrals are evaluated using the tables in Gradshteyn and Ryzhik[1], validated numerically and reproduced in supplementary material. References to equations are given as GR(X), where X corresponds to the number of the identity in the original tables.

Supporting simulation for derivation

Each of the analytically derived frequency shifts derived below are presented with a simple computer simulation to demonstrate the results. Figure S1 gives an overview of the microstructure used for the simulation. We constructed a multilayer cylinder in a 3D grid with dimensions $L^3 = 600^3$ grid units. The cylinder consisted of four layers with radii $R_1 = 30$, $R_2 = 50$, $R_3 = 70$, $R_4 = 90$ grid units and cylinder length L. Randomly positioned dots (diameter of 1 grid units) were placed in each of the three water compartments, with a total density ε ranging from approximately 1% to 20%. Using the discrete Fourier transform with periodic boundary conditions, we computed the k-space indicator function for the cylinder, and for each population of spheres. Using Eqs. (3)-(4) we could numerically compute a ground truth Lorentzian tensors $\mathbf{L}$ from combinations of indicator functions and magnetic susceptibility in k-space. These results were compared with the analytical results derived below to validate our results.
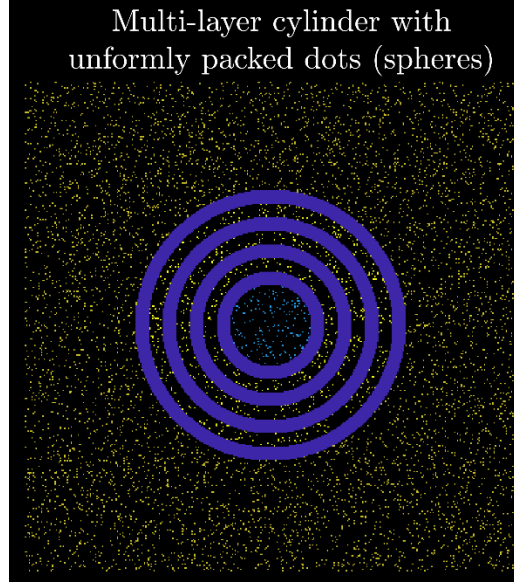
Figure S1 - Simulation of multi-layer cylinder and spheres: A 4-layers cylinder are packed in a 3D grid, with uniformly packed dots in all its compartments. Extra-cylindrical dots are shown here in orange, bilayers in purple and intra in cyan. While the dots are uniformly distributed in each compartment, they are still restricted by the presence of the cylinder, which generates a structural anisotropy in their positions.

S1) Contribution from cylinders with orientation dispersion and susceptibility anisotropy $\Delta\chi$

Here we focus on deriving the Lorentzian tensor $\mathbf{L}$ (cf. Eq. (3)), purely from the population of infinitely long cylinders with arbitrary orientations. Their directions are assumed to be independent of their size and randomly positioned. Each cylinder consists of multiple concentric shells with an associated axially symmetric microscopic susceptibility tensor χ^{C} which describes the microscopic content of lipid-protein chains, phospholipid channels etc. as written in Eq. (11).

The Lorentzian tensor $\mathbf{L}$, where we implicitly know that cylinders are both target and source is

$$\mathbf{L} = -\frac{1}{\zeta^{\mathrm{W}}} \int \frac{d\boldsymbol{k}}{(2\pi)^3} \boldsymbol{\Upsilon}(\boldsymbol{k}) \boldsymbol{\Gamma}(\boldsymbol{k}). \tag{S1}$$

Here ζ^{W} denotes the total water volume fraction outside of all inclusion types (cylinders of total volume fraction ζ^{C} and spheres with a total volume fraction ζ^{S}). Equation (S1) depends on the tensor-valued cross-correlation tensor $\boldsymbol{\Gamma}(\boldsymbol{k})$ for cylinders

$$\Gamma(\boldsymbol{k}) = \frac{v^{C}(\boldsymbol{k})\chi^{C}(-\boldsymbol{k})}{|\mathcal{M}|} - (2\pi)^{3}\zeta^{C}\overline{\chi}^{C}\delta(\boldsymbol{k}), \text{(cylinder correlation function)}, \tag{S2}$$

where $v^{C}(\boldsymbol{k})$ and $\chi^{C}(\boldsymbol{k})$ is the structural indicator function and magnetic susceptibility of all the cylinders in k-space, and $\overline{\chi}^{C}$ is the mesoscopically averaged magnetic susceptibility tensor. The first step in computing $\mathbf{L}$ is to determine $\Gamma(\boldsymbol{k})$, Eq. (S2), by finding its constituents. We start by re-visiting[2] the k-space indicator function $v^{C}(\boldsymbol{k})$ and its mean ζ^{C}, and then proceed to derive the magnetic susceptibility $\chi^{C}(\boldsymbol{k})$ and mesoscopically averaged (bulk) susceptibility $\overline{\chi}^{C}$.

Indicator function of cylinders $v^{C}(\boldsymbol{k})$

Positions $\boldsymbol{r}$ within an infinitely long cylinder solid cylinder with radius R displaced $\boldsymbol{u} = u\hat{\boldsymbol{u}}$ from the origin can be parametrized by [2]

$$\boldsymbol{r} = (u + r\cos(\phi))\hat{\boldsymbol{u}} + r\sin(\phi)\hat{\boldsymbol{v}} + s\hat{\boldsymbol{n}}, \tag{S3}$$

where $\hat{\boldsymbol{n}}$ is a unit vector along the cylinder axis and $\hat{\boldsymbol{v}}$, $\hat{\boldsymbol{n}}$ and $\hat{\boldsymbol{u}}$ are mutually perpendicular. Hence, (r, ϕ, s) become local cylinder coordinates (listed here for later convenience). We have previously derived the indicator function for an infinitely long solid cylinder[2,3]. The indicator function $v(\boldsymbol{k})$ of a single infinitely long solid cylinder is found previously to be

$$\begin{aligned} v(\boldsymbol{k}) &= e^{i\boldsymbol{k}\cdot\boldsymbol{u}}\frac{4\pi^{2}}{k}RJ_{1}(Rk)\delta(\boldsymbol{k}\cdot\hat{\boldsymbol{n}}), \quad \text{(infinitely long cylinder)}, \\ &= e^{i\boldsymbol{k}\cdot\boldsymbol{u}}v^{2D}(\boldsymbol{k})2\pi\delta(\boldsymbol{k}\cdot\hat{\boldsymbol{n}}), \end{aligned} \tag{S4}$$

where

$$v^{2D}(k) = \frac{2\pi}{k}RJ_{1}(Rk) \tag{S5}$$

is the 2D indicator function of the cylinder cross-section. R denotes the radii of the cylinder. The volume fraction of the infinite cylinder is understood as $\zeta_{1} = 2\pi LR^{2}/|\mathcal{M}|$, $L \to \infty$, given as the limit

of a cylinder of length 2L going to infinity. The indicator function $v^C(\mathbf{k})$ of all cylinders is then simply the sum $v^C(\mathbf{k}) = \sum_q v_q(\mathbf{k})$ over all individual cylinders labelled by the index q.

Magnetic susceptibility of a cylinder $\chi^C(\mathbf{k})$

Consider a lipid forming part of the myelin associated with the cylinder. The lipid is perpendicular to $\hat{\mathbf{n}}$ and form an angle ϕ to $\hat{\mathbf{u}}$. The direction of the lipid is $\hat{\mathbf{v}}_1 = \cos(\phi)\hat{\mathbf{u}} + \sin(\phi)\hat{\mathbf{v}}$. Hence, $\hat{\mathbf{v}}_1$ is the eigenvector of $\boldsymbol{\chi}$ associated with parallel susceptibility $\chi^{\parallel}$ in Eq. (11), whereas the perpendicular vectors to the lipid $\hat{\mathbf{v}}_2 = -\sin(\phi)\hat{\mathbf{u}} + \cos(\phi)\hat{\mathbf{v}}$ and $\hat{\mathbf{n}}$ are the eigenvectors corresponding to $\chi_{\perp}$. Thus, the susceptibility of a lipid inside a cylinder placed at origo is

$$
\begin{aligned}
\chi(\phi) &= \chi_{\parallel}\hat{\mathbf{v}}_1\hat{\mathbf{v}}_1^{\mathrm{T}} + \chi_{\perp}\left(\hat{\mathbf{v}}_2\hat{\mathbf{v}}_2^{\mathrm{T}} + \hat{\mathbf{n}}\hat{\mathbf{n}}^{\mathrm{T}}\right) \\
&= \left(\chi^C - \frac{1}{3}\Delta\chi\right)\mathbf{I} + \Delta\chi\left(\cos^2(\phi)\hat{\mathbf{u}}\hat{\mathbf{u}}^{\mathrm{T}} + \sin^2(\phi)\hat{\mathbf{v}}\hat{\mathbf{v}}^{\mathrm{T}} + \cos(\phi)\sin(\phi)\left(\hat{\mathbf{v}}\hat{\mathbf{u}}^{\mathrm{T}} + \hat{\mathbf{u}}\hat{\mathbf{v}}^{\mathrm{T}}\right)\right)^{\text{(cylinder frame)}}
\end{aligned}
$$

$$\text{(S6)}$$

where we introduced

$$
\chi^C \equiv \frac{\chi^{\parallel} + 2\chi^{\perp}}{3} = \frac{1}{3}\mathrm{Tr}(\chi) \text{ and } \Delta\chi = \chi^{\parallel} - \chi^{\perp}. \tag{S7}
$$

It will prove convenient to rewrite $\chi(\phi)$ as

$$
\chi(\phi) = \chi_0 + \mathrm{Re}\left\{\chi_2 e^{2i\phi}\right\} = \chi_0 + \frac{1}{2}\left(\chi_2 e^{2i\phi} + c.c\right). \tag{S8}
$$

Where c.c. denotes the complex conjugation of the second complex term, and χ_0, χ_2 are the only non-zero coefficient matrices of $\chi(\phi)$ Fourier series

$$
\chi_0 = \chi^C\mathbf{I} + \frac{1}{2}\Delta\chi\left(\frac{1}{3}\mathbf{I} - \hat{\mathbf{n}}\hat{\mathbf{n}}^{\mathrm{T}}\right) \tag{S9}
$$

and

$$
\chi_2 = \frac{\Delta\chi}{2}\left(\hat{\mathbf{u}}\hat{\mathbf{u}}^{\mathrm{T}} - \hat{\mathbf{v}}\hat{\mathbf{v}}^{\mathrm{T}} - i\left(\hat{\mathbf{u}}\hat{\mathbf{v}}^{\mathrm{T}} + \hat{\mathbf{v}}\hat{\mathbf{u}}^{\mathrm{T}}\right)\right). \tag{S10}
$$

4

Having obtained the susceptibility for a single lipid in the myelin sheath, the magnetic susceptibility of the whole myelin sheath $\chi^C(\mathbf{k})$ can be determined by multiplying Eq. (S8) with the cylinder indicator function $v(\mathbf{k})$, Eq. (S4). For a solid cylinder, the susceptibility in k-space becomes

$$\chi^C(\mathbf{k}) = 2\pi\delta(\mathbf{k}\cdot\hat{\mathbf{n}})e^{iuk\cdot\hat{u}}\int_0^R d\rho\rho\int_0^{2\pi} d\phi\, e^{i\rho k\cos(\psi-\phi)}\left(\chi_0 + \text{Re}\{\chi_2 e^{2i\phi}\}\right). \tag{S11}$$

Here we used $\hat{\mathbf{k}}\cdot\hat{\mathbf{u}} = \cos(\psi)$, $\hat{\mathbf{k}}\cdot\hat{\mathbf{v}} = \sin(\psi)$. The radial integral of Eq. (S11) is

$$\int_0^R d\rho\rho\int_0^{2\pi} d\phi\, e^{im\phi + ik\rho\cos(\phi-\psi)} = 2\pi\int_{r_q}^{R_q} dr\, r\, e^{im(\psi - \pi/2)}J_m(kr)$$

$$= 2\pi e^{im\psi}\begin{cases} \dfrac{RJ_1(Rk)}{k}, & m = 0 \\[3mm] \dfrac{2 - 2J_0(kR) - kRJ_1(kR)}{k^2}, & m = \pm 2 \end{cases} \tag{S12}$$

$$\equiv 2\pi e^{im\psi}\begin{cases} \xi_0(kR), & m = 0 \\ \xi_2(kR), & m = \pm 2 \end{cases}$$

Here we see that $v^{2D}(\mathbf{k}) = 2\pi\xi_0(Rk)$. Having established all the components of $\chi^C(\mathbf{k})$, the k-space magnetic susceptibility of a solid cylinder becomes

$$\chi^C(\mathbf{k}) = \chi_0 v^C(\mathbf{k}) - 4\pi^2\delta(\mathbf{k}\cdot\hat{\mathbf{n}})\text{Re}\{\chi_2 e^{2i\psi}\}\xi_2(kR), \text{ (solid cylinder).} \tag{S13}$$

Finding the magnetic susceptibility for a cylinder displaced $\mathbf{u}$, consisting of multiple concentric shells is straightforward, as it follows directly from the shift theorem of the Fourier transform and the superposition principle, respectively, where positions ρ within the q'th layer are denoted by the layer radii $r_q < \rho < R_q$:

$$\chi^C(\mathbf{k}) = 4\pi^2\delta(\mathbf{k}\cdot\hat{\mathbf{n}})e^{ik\cdot u}\left\{\chi_0\sum_q\left(\xi_0(kR_q) - \xi_0(kr_q)\right)\right.$$
$$\left. - \text{Re}\{\chi_2 e^{2i\psi}\}\sum_q\left(\xi_2(kR_q) - \xi_2(kr_q)\right)\right\}, \text{ (multi-layered cylinder).} \tag{S14}$$

Similarly, we can sum Eq. (S14) for multiple cylinders with different orientations $\hat{\mathbf{n}}$ and distributions of radii, assumed to be independent of each other. The mean (bulk) susceptibility $\overline{\chi}^C$ of Eq. (S14) within $\mathcal{M}$ is given by its value at $k = 0$

$$\bar{\chi}^C = \frac{1}{|\mathcal{M}|}\chi^C(k=0) = \chi_0\zeta_1.$$

(S15)

Contribution to Lorentzian tensor from autocorrelation of cylinders

For simplicity we start by calculating the contribution to the Lorentzian tensor $\mathbf{L}$ from the autocorrelation of two cylinders, describing the mean of the self-generated Larmor frequency shift

$$-\frac{1}{\zeta^W}\int\frac{d\boldsymbol{k}}{(2\pi)^3}\Upsilon(\boldsymbol{k})\delta(\boldsymbol{k}\cdot\hat{\boldsymbol{n}})\left\{8\pi^2\sum_{q'}\left(\frac{\zeta_{R_{q'}}}{R_{q'}}J_1(kR_{q'})-\frac{\zeta_{r_{q'}}}{r_{q'}}J_1(kr_{q'})\right)\cdot\left(\boldsymbol{\chi}_0\sum_q\left(\xi_0(kR_q)-\xi_0(kr_q)\right)\right.\right.$$
$$\left.-\operatorname{Re}\{\boldsymbol{\chi}_2 e^{2i\psi}\}\sum_q\left(\xi_2(kR_q)-\xi_2(kr_q)\right)\right)$$
$$\left.-4\pi^2\frac{\delta(k)}{k}\zeta_1\bar{\boldsymbol{\chi}}_0\right\}$$

(S16)

The volume fraction ζ_R is of a solid cylinder with radius R. Eq. (S16) consists of three parts, where the second part depends on ψ. We start by looking at the first and third contribution as they are exactly what was considered in our previous study[2], but here we have the tensor susceptibility $\boldsymbol{\chi}_0$ instead of a scalar. The first and third term are thus

$$\frac{\zeta_1(1-\zeta_1)}{\zeta^W}\frac{1}{2}\left(\hat{\boldsymbol{n}}\hat{\boldsymbol{n}}^T-\frac{1}{3}\mathbf{I}\right)\boldsymbol{\chi}_0 = \frac{\zeta_1(1-\zeta_1)}{\zeta^W}\left\{\frac{1}{2}\left(\hat{\boldsymbol{n}}\hat{\boldsymbol{n}}^T-\frac{1}{3}\mathbf{I}\right)\chi^C\mathbf{I}-\frac{1}{12}\Delta\chi\left(\hat{\boldsymbol{n}}\hat{\boldsymbol{n}}^T+\frac{1}{3}\mathbf{I}\right)\right\}.$$

(S17)

Left to solve is the ψ-dependent term in Eq. (S16). The angular integration can be carried out by rewriting the dipole kernel into trigonometric functions in the eigenspace of the cylinder

$$\int\frac{d\psi}{\pi}\left(\frac{1}{3}\mathbf{I}-\cos^2(\psi)\hat{\boldsymbol{u}}\hat{\boldsymbol{u}}^T-\sin^2(\psi)\hat{\boldsymbol{v}}\hat{\boldsymbol{v}}^T-\cos(\psi)\sin(\psi)\left(\hat{\boldsymbol{v}}\hat{\boldsymbol{u}}^T+\hat{\boldsymbol{u}}\hat{\boldsymbol{v}}^T\right)\right)\operatorname{Re}\{\boldsymbol{\chi}_2 e^{2i\psi}\} = \frac{\Delta\chi}{2}\left(\hat{\boldsymbol{n}}\hat{\boldsymbol{n}}^T-\mathbf{I}\right).$$

(S18)

What is left to calculate is the radial integral for a single cylinder defined as λ_1

$$\lambda_1 \equiv -\frac{6}{\zeta^W\zeta^C}\int dk\,k\sum_{q,q'}\left(\frac{\zeta_{R_{q'}}}{R_{q'}}J_1(kR_{q'})-\frac{\zeta_{r_{q'}}}{r_{q'}}J_1(kr_{q'})\right)\left(\xi_2(kR_q)-\xi_2(kr_q)\right).$$

(S19)

The parameter λ_1 describes the layer geometry of the cylinder. We have added -6 to ensure λ_1 is positive and so its contribution to the Lorentzian tensor is weighted similar to Eq. (S17). Using Eq. (S12) for ξ_2 and the integral expressions (which follows from GR(6.533.3) and GR(6.573.(1-2)))

$$\int dk \left(J_1(xk) \right) \frac{2 - 2J_0(ky) - kyJ_1(ky)}{k^2} = \begin{cases} x \ln \left(\dfrac{y}{x} \right), & y > x \\ 0, & y \leq x \end{cases} \tag{S20}$$

we obtain

$$\lambda_1 = -\frac{6}{\zeta^W \zeta^C} \left(\sum_{q>q'} \left(\zeta_{R_{q'}} - \zeta_{r_{q'}} \right) \ln \left(\frac{R_q}{r_q} \right) - \sum_q \zeta_{r_q} \ln \left(\frac{R_q}{r_q} \right) \right). \tag{S21}$$

Collecting all the results we obtain for the auto-correlation contribution to $\mathbf{L}$ from a single cylinder

$$-\frac{\zeta_1 (1 - \zeta_1)}{\zeta^W} \left\{ \frac{1}{2} \left(\hat{\boldsymbol{n}} \hat{\boldsymbol{n}}^{\mathrm{T}} - \frac{1}{3} \mathbf{I} \right) \chi^C \mathbf{I} - \frac{1}{12} \Delta \chi \left(\hat{\boldsymbol{n}} \hat{\boldsymbol{n}}^{\mathrm{T}} + \frac{1}{3} \mathbf{I} \right) \right\} - \zeta_1 \frac{\Delta \chi}{12} \lambda_1 \left(\hat{\boldsymbol{n}} \hat{\boldsymbol{n}}^{\mathrm{T}} - \mathbf{I} \right), \text{ (single cylinder).} \tag{S22}$$

Contribution to Lorentzian tensor from cross-correlation of cylinders

Left to consider is the contribution to the Lorentzian tensor, Eq. (S1), from cross-correlations between a pair of different cylinders, i.e., the mean frequency shift inside a cylinder generated by a neighboring cylinder. Fortunately, we have previously shown that such a contribution can be neglected when the magnetic susceptibility of the cylinders is scalar. Second, it is well known from previous studies[4,5] that the functional form of the induced field from a cylinder with a radially symmetric tensor susceptibility anisotropy, as described by Eq. (S6), does not change external to the cylinders. This means that our previous results on considering the contribution from cross-correlations are valid here, as two cylinders are always external to each other. We can therefore neglect an explicit calculation (however, we did calculate it explicitly to verify this).

Total Lorentzian tensor from cylinders as targets and sources

Summing over N cylinders, and using $\mathbf{T} = \sum_j \hat{\boldsymbol{n}}\hat{\boldsymbol{n}}^{\mathrm{T}} / N$ is the fODF scatter matrix of the cylinders, and impose the distribution of orientations is independent of their distribution in size, we find the Lorentzian tensor from all the cylinders being targets and sources to be

$$\mathbf{L} = -\frac{\zeta^C \left(1 - \zeta^C\right)}{\zeta^{\mathrm{W}}} \left\{ \frac{1}{2}\left(\mathbf{T} - \frac{1}{3}\mathbf{I}\right)\chi^C\mathbf{I} - \frac{1}{12}\Delta\chi\left(\mathbf{T} + \frac{1}{3}\mathbf{I}\right) \right\} - \zeta^C \frac{\Delta\chi}{12}\lambda^C\left(\mathbf{T} - \mathbf{I}\right), \text{ (multiple cylinders).}$$

(S23)

Here we defined $\zeta^C = N\langle\zeta_1\rangle$ as N times the average cylinder volume fraction $\langle\zeta_1\rangle$, and similar $\lambda^C = N\langle\lambda_1\rangle$.

S2) Lorentzian tensor from spherical inclusions

Next, we derive the mesoscopic contribution from different populations of solid spherical inclusions. For simplicity, we assume that every cylindrical water compartment, i.e., extra-axonal (E), bi-layers (M) and intra-axonal (A), contains a population of spherical inclusions whose size are independent of their positions, The total indicator function of all spheres in k-space is denoted $v^{\mathrm{S}}(\boldsymbol{k})$, their volume fraction $\zeta^S = \zeta^{\mathrm{E}} + \zeta^{\mathrm{M}} + \zeta^{\mathrm{A}}$, and their total magnetic susceptibility $\chi^{\mathrm{S}}(\boldsymbol{k}) = \chi^{\mathrm{A}}(\boldsymbol{k}) + \chi^{\mathrm{M}}(\boldsymbol{k}) + \chi^{\mathrm{E}}(\boldsymbol{k})$. We assume that each population is uniformly positioned within each compartment. Hence, they are positionally restricted by the cylinders especially when their volume fraction increases. Since χ^{S} is a scalar, we only have to consider the demagnetization tensor $\mathbf{N}$

$$\mathbf{N} = \frac{1}{\zeta^{\mathrm{W}}} \int \frac{d\boldsymbol{k}}{(2\pi)^3} \Upsilon(\boldsymbol{k})\Gamma(\boldsymbol{k}),$$

(S24)

which depends on the scalar-valued structure-structure correlation function $\Gamma(\boldsymbol{k})$ of all spheres

$$\Gamma(\boldsymbol{k}) = \frac{v^{\mathrm{S}}(\boldsymbol{k})v^{\mathrm{S}}(-\boldsymbol{k})}{|\mathcal{M}|}.$$

(S25)

For spheres we do not need to care about the singular point of $\Gamma(\boldsymbol{k})$ at $k = 0$, as this term integrates to zero. The generic indicator function $v(\boldsymbol{k})$ for a single sphere of radius R positioned at $u\hat{\boldsymbol{u}}$ from the origin can be found using the following vector $\boldsymbol{r}$ on a spherical surface of radius r

$$r(r,\varphi,\vartheta) = \hat{u}u + \hat{r}r + \hat{\vartheta}\vartheta r + r\sin(\theta)\varphi\hat{\varphi}. \tag{S26}$$

Here $(\hat{r},\hat{\vartheta},\hat{\varphi})$ is the unit spherical vectors so (r,ϑ,φ) become local coordinates in the sphere. The indicator function $v(\boldsymbol{k})$ becomes

$$v(\boldsymbol{r}) = \int_0^R dr'\, r'^2 \int_0^\pi d\vartheta \sin(\vartheta) \int_0^{2\pi} d\varphi\, \delta(\boldsymbol{r} - \hat{u}u - \hat{r}r' - \hat{\vartheta}\vartheta r' - r'\sin(\theta)\varphi\hat{\varphi}), \tag{S27}$$

and in k-space

$$v(\boldsymbol{k}) = \int d\boldsymbol{k}\, e^{i\boldsymbol{k}\cdot\boldsymbol{r}} \int_0^R dr'\, r'^2 \int_0^\pi d\vartheta \sin(\vartheta) \int_0^{2\pi} d\varphi\, \delta(\boldsymbol{r} - \boldsymbol{u} - \hat{r}r' - \hat{\vartheta}\vartheta r' - r'\sin(\theta)\varphi\hat{\varphi})$$
$$= e^{i\boldsymbol{k}\cdot\boldsymbol{u}} 4\pi R^2 \frac{j_1(kR)}{k}, \text{(single sphere)}. \tag{S28}$$

Notice that the indicator function for a single sphere only has angular dependence in the exponential describing its positions $\boldsymbol{u}$. This means that the autocorrelation function in k-space $v(\boldsymbol{k})v(-\boldsymbol{k})/|\mathcal{M}|$ of a sphere has no angular dependence, since the exponentials cancel. Therefore, when calculating the contribution to $\mathbf{N}$ from sphere's autocorrelations, the angular integration in Eq. (S28) is exclusively over the dipole kernel, which integrates to zero, i.e.

$$\int d\hat{k}\, \Upsilon(\hat{\boldsymbol{k}}) = 0. \tag{S29}$$

Hence, no frequency shift is associated with autocorrelation from the spheres.

Left to consider is the contribution to $\mathbf{N}$ from cross-correlations $v_1(\boldsymbol{k})v_2(-\boldsymbol{k})/|\mathcal{M}|$ between all possible pairs of spheres in every population. For simplicity, consider the contribution to $\mathbf{N}$ from the cross-correlation between two distinct spheres with radius R_1 and R_2 separated a distance $\Delta\boldsymbol{u} = \boldsymbol{u}_1 - \boldsymbol{u}_2$

$$\frac{1}{\zeta^{\mathrm{W}}} \frac{2(R_1 R_2)^2}{\pi|\mathcal{M}|} \int d\boldsymbol{k}\, \Upsilon(\boldsymbol{k}) e^{i\boldsymbol{k}\cdot\Delta\boldsymbol{u}} \frac{j_1(kR_1)\, j_1(kR_2)}{k^2}, \text{(two spheres)}. \tag{S30}$$

As the angular dependence of Eq. (S30) is captured only by the displacement $e^{i\boldsymbol{k}\cdot\Delta\boldsymbol{u}}$, it is convenient to rewrite it in terms of a plane wave expansion[6]

$$e^{i\boldsymbol{k}\cdot\Delta\boldsymbol{u}} = 4\pi \sum_l \sum_{m=-l}^l i^l j_l(k\Delta u) Y_l^{m*}(\Delta\hat{\boldsymbol{u}}) Y_l^m(\hat{\boldsymbol{k}}). \tag{S31}$$

Furthermore, it will be convenient to rewrite the dipole kernel (k-space) and dipole field (real space) in terms of spherical harmonics Y_2^m and STF tensors $\mathcal{Y}_{2m}$ [7]

$$\Upsilon(\boldsymbol{k}) = -\frac{8\pi}{15}\sum_{m=-2}^{2}\mathcal{Y}_{2m}Y_2^m(\hat{\boldsymbol{k}}), \text{ (k-space)}, \quad \Upsilon(\boldsymbol{r}) = \frac{6}{15}\frac{1}{r^3}\sum_{m=-2}^{2}\mathcal{Y}_{2m}Y_2^m(\hat{\boldsymbol{r}}), \text{ (real space). (S32)}$$

Using the orthonormality of spherical harmonics, the angular integral of Eq. (S30) is

$$\int d\hat{\boldsymbol{k}}\,\Upsilon(\boldsymbol{k})e^{i\boldsymbol{k}\cdot\Delta\boldsymbol{u}} = -\frac{32\pi^2}{15}\sum_{m'=-2}^{2}\mathcal{Y}_{2m'}\sum_{l}i^l j_l(k\Delta u)\sum_{m=-l}^{l}Y_l^{m*}(\Delta\hat{\boldsymbol{u}})\int d\hat{\boldsymbol{k}}\,Y_2^{m'}(\hat{\boldsymbol{k}})Y_l^m(\hat{\boldsymbol{k}})$$

$$= 4\pi j_2(k\Delta u)\left(\Delta\hat{\boldsymbol{u}}\Delta\hat{\boldsymbol{u}}^{\mathrm{T}} - \frac{1}{3}\mathbf{I}\right). \tag{S33}$$

Using GR(6.573.1), the radial integration of Eq. (S30) is

$$\int dk\, j_1(kR_1)\,j_1(kR_2)\,j_2(k\Delta u) = \frac{\pi}{6}R_1 R_2\left(\frac{1}{\Delta u}\right)^3 \tag{S34}$$

Combining Eqs. (S32)-(S34), the contribution to $\mathbf{N}$ from the cross-correlations between two distinct spheres are

$$\mathbf{N} = \frac{V_1 V_2}{\zeta^{\mathrm{W}}|\mathcal{M}|}\Upsilon(\Delta\boldsymbol{u}), \text{ (two spheres)}, \tag{S35}$$

where $V_1 = 4\pi R_1^3/3$ is the first sphere's volume and $\Upsilon(\Delta\boldsymbol{u})$ is the dipole field in real space. Eq. (S35) tells us that the mean field induced in a sphere from a neighboring sphere is proportional to the elementary dipole field and scaled by the volumes of the spheres. This is luckily expected since the only non-zero term of the multipole expansion of the field from a sphere is the dipolar term.

The next step is to sum over all these dipolar fields between every sphere in $\mathcal{M}$. However, it is in general highly impractical to sum Eq. (S35), whenever spheres are not Poissonian distributed in the whole mesoscopic region $\mathcal{M}$. To proceed, assumptions must be made about the restrictions in positions of spheres in correspondence with the desired model picture. If the spheres are uniformly positioned in a given water compartment, we do not need to account for every position of the spheres, so long as the spheres are smaller than the size of the water compartments - only the shape of the compartment in which they reside. This allows us to smooth the positions of the spherical inclusions

(similar to what is done in QSM on the macroscopic scale). We therefore represent a discrete sum of spheres in a given water compartment by an indicator function $\tilde{v}(r)$ for the whole occupying space

$$v(r) \rightarrow \tilde{v}(r)\varepsilon, \text{ (Coarse grained indicator function)}, \tag{S36}$$

where $\varepsilon = \zeta / \tilde{\zeta}$ is the density of spheres that normalizes the indicator function so upon integration it has the original volume fraction ζ of the spheres, instead of the volume fraction $\tilde{\zeta}$ occupied by the coarse-grained indicator function $\tilde{v}(r)$. For example, the sum over all intra-axonal spheres are represented by the indicator function describing the whole intra-axonal compartment and then scaled by the density of intra-axonal spheres. In fact, this approximation is exactly what we employed when defining the indicator function of the lipid chains forming the cylinders. There, the density factor was just absorbed into the microscopic susceptibility tensor $\boldsymbol{\chi}^{C}$, Eq. (11), for the cylinder layers. Hence, when considering the contribution to $\mathbf{N}$ from the cross-correlations between two populations of spheres, we make the approximation

$$
\begin{aligned}
\mathbf{N} &= \sum_{qq'} \frac{\varepsilon_q \varepsilon_{q'}}{\zeta^{\mathrm{W}}} \int \frac{d\boldsymbol{k}}{(2\pi)^3} \Upsilon(\boldsymbol{k}) \frac{v_q(\boldsymbol{k}) v_{q'}(-\boldsymbol{k})}{|\mathcal{M}|} \\
&\simeq \frac{\varepsilon_1 \varepsilon_2}{\zeta^{\mathrm{W}}} \int \frac{d\boldsymbol{k}}{(2\pi)^3} \Upsilon(\boldsymbol{k}) \frac{\tilde{v}_1(\boldsymbol{k}) \tilde{v}_2(-\boldsymbol{k})}{|\mathcal{M}|}
\end{aligned}
\text{, (two populations of spheres)}. \tag{S37}
$$

Here $\tilde{v}_1(\boldsymbol{k})$ is understood as the coarse-grained indicator function of the first population with density ε_1 etc. When $\tilde{v}_1(\boldsymbol{k}) = \tilde{v}_2(\boldsymbol{k})$, we can think of Eq. (S37) as an autocorrelation between the two populations of spheres (not to be confused with autocorrelation between distinct spheres). All the coarse-grained compartments can be written in terms of cylindrical indicator functions, which makes it easy to calculate $\mathbf{N}$, Eq. (S37). For example, the coarse-grained indicator function of extra-axonal spheres can be written as $\tilde{v}(r) = 1 - v^{\mathrm{SC}}(r)$, i.e. determined by the indicator function of all the cylinders (here assumed to be solid and thus indicated by $v^{\mathrm{SC}}(r)$ with volume fraction ζ^{SC} to distinguish from hollowed cylinders).

The demagnetization tensors describing the cross contributions between the same population of spheres are

$$\mathbf{N} = \frac{\zeta_1^2}{\zeta^W} \frac{1-\tilde{\zeta}_1}{\tilde{\zeta}_1} \frac{1}{2} \left(\mathbf{T} - \frac{1}{3}\mathbf{I} \right), \text{ (identical populations)} \tag{S38}$$

Figure S2 shows a good agreement between Eq. (S38) to our simulation (see description in the beginning of the supporting material) for each demagnetization tensor contribution between identical populations of intra-axonal spheres (A), spheres in MW (M) or extra-axonal spheres (E), respectively.

Similarly, the demagnetization tensors from cross contributions between different populations of spheres are

$$\mathbf{N} = -\frac{\zeta_1 \zeta_2}{\zeta^W} \frac{1}{2} \left(\mathbf{T} - \frac{1}{3}\mathbf{I} \right), \text{ (different populations).} \tag{S39}$$

Figure S3 shows a good agreement between Eq. (S39) to our simulation (see description in the beginning of supporting material) for each demagnetization tensor contribution between different populations of intra-axonal spheres (A), spheres in MW (M) or extra-axonal spheres (E), respectively.
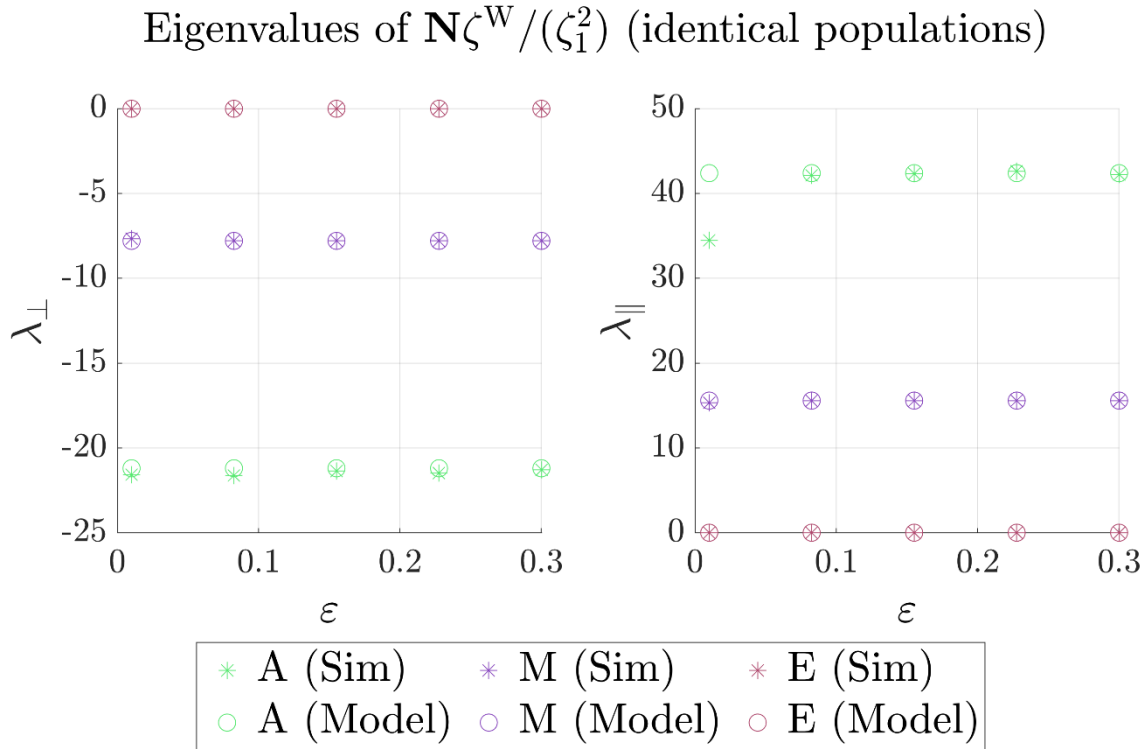
Eigenvalues of $\mathbf{N}\zeta^W/(\zeta_1^2)$ (identical populations)

Figure S2 - Demagnetization tensor eigenvalues from cross-correlations between identical populations of spheres: Here the target and source are from the same population of spheres. The left figure shows the average perpendicular eigenvalue $\lambda_\perp$, and the right figure shows the parallel $\lambda_\parallel$, wrt. to the axes of the cylinder. The x-axis shows the density ε of spheres in a given water compartment.
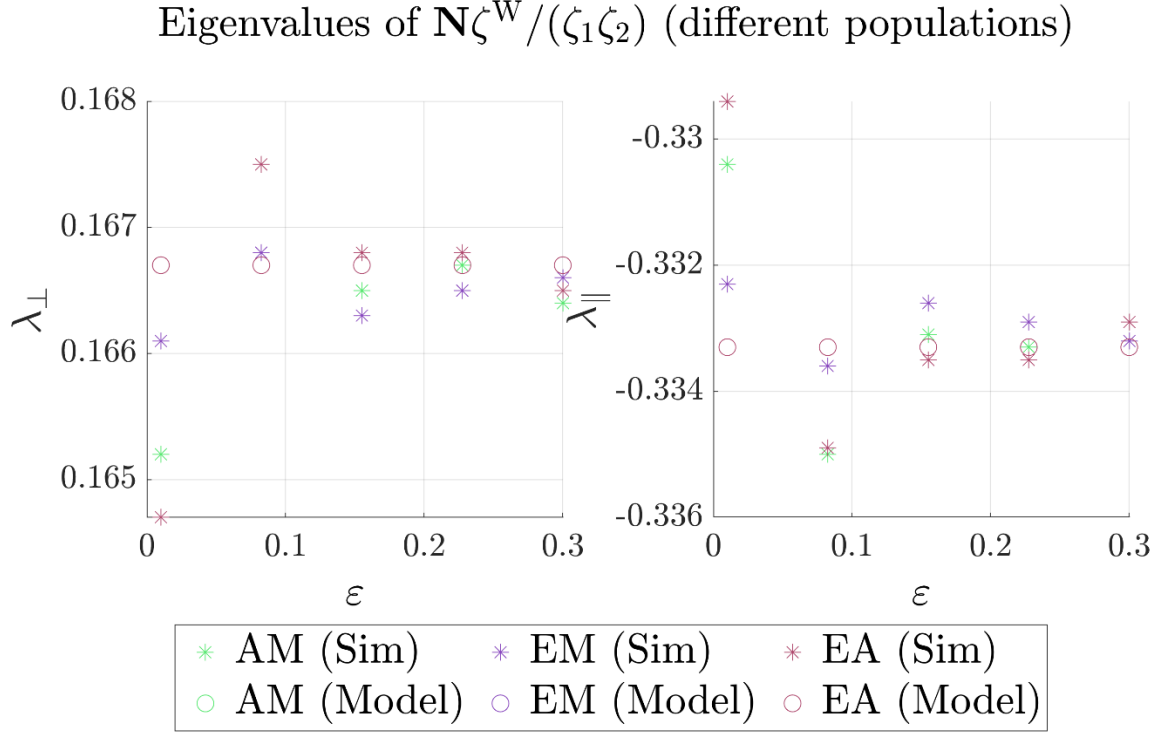
Figure S3 - Demagnetization tensor eigenvalues from cross-correlations between different populations of spheres: Here the target and source are different populations of spheres. The left figure shows the average perpendicular eigenvalue $\lambda_\perp$, and the right figure shows the parallel $\lambda_\parallel$, wrt. to the axes of the cylinder. The x-axis shows the density ε of spheres in a given water compartment.

S3) Lorentizian tensor from cross-correlations between spherical and cylindrical inclusions

In this section we derive the contribution from cross-correlations between cylindrical and spherical inclusions. Since the cylinders have susceptibility anisotropy, the cross-correlation differs from the induced field from spheres and averaged within the cylinders. We therefore start by considering the demagnetization tensor $\mathbf{N}$ for when spherical inclusions are sources and the cylinders are targets, and then vice versa.

Demagnetization tensor from spherical sources and cylindrical targets

Consider the demagnetization tensor from a single cylinder layer with radii r_1, R_1 and a sphere of radius R_2 placed at the origin. The cylinder is considered as the target and the sphere generates the field. This demagnetization tensor is described by the scalar-valued cross-correlation function $\Gamma(\boldsymbol{k})$

$$\Gamma(\boldsymbol{k}) = e^{iku\cos(\psi)}\frac{12\pi^2}{k^2}\left(\xi_0(R_1k)-\xi_0(r_1k)\right)\zeta_2\frac{j_1(kR_2)}{R_2}\delta(\boldsymbol{k}\cdot\hat{\boldsymbol{n}})$$
$$-4\pi^2\zeta_1\zeta_2\frac{\delta(\boldsymbol{k}\cdot\hat{\boldsymbol{n}})\delta(k)}{k} \quad \text{, (cylinder target, sphere source),}$$

(S40)

where $\boldsymbol{k}\cdot\boldsymbol{u} = ku\cos(\psi)$. The corresponding contribution to the demagnetization tensor is

$$3\frac{\zeta_2}{\zeta^W R_2}\int dk\int\frac{d\hat{\boldsymbol{k}}}{2\pi}\left\{\frac{1}{k}\left(\xi_0(R_1k)-\xi_0(r_1k)\right)j_1(kR_2)\Upsilon(\hat{\boldsymbol{k}})\delta(\boldsymbol{k}\cdot\hat{\boldsymbol{n}})e^{iku\cos(\psi)}\right.$$
$$\left. -4\pi^2\zeta_1\zeta_2\frac{\delta(\boldsymbol{k}\cdot\hat{\boldsymbol{n}})\delta(k)}{k}\right\}$$

(cylinder target, sphere source).

(S41)

We start by calculating the first ψ-dependent term of Eq. (S41). Rewriting $\Upsilon(\hat{\boldsymbol{k}})$ in terms of trigonometric functions in the basis of the cylinder layer, the angular integral of Eq. (S41) is found to be

$$\int\frac{d\psi}{2\pi}\left(\frac{1}{3}\mathbf{I}-\cos^2(\psi)\hat{\boldsymbol{u}}\hat{\boldsymbol{u}}^{\mathrm{T}}-\sin^2(\psi)\hat{\boldsymbol{v}}\hat{\boldsymbol{v}}^{\mathrm{T}}-\cos(\psi)\sin(\psi)\left(\hat{\boldsymbol{v}}\hat{\boldsymbol{u}}^{\mathrm{T}}+\hat{\boldsymbol{u}}\hat{\boldsymbol{v}}^{\mathrm{T}}\right)\right)e^{iku\cos(\psi)}$$
$$=\left(\frac{1}{3}\mathbf{I}-\hat{\boldsymbol{u}}\hat{\boldsymbol{u}}^{\mathrm{T}}\right)J_0(ku)+\left(\hat{\boldsymbol{u}}\hat{\boldsymbol{u}}^{\mathrm{T}}-\hat{\boldsymbol{v}}\hat{\boldsymbol{v}}^{\mathrm{T}}\right)J_1(ku)\frac{1}{ku}$$

(S42)

The radial integral left to solve is

$$\int dk\frac{1}{k}\left(\xi_0(R_1k)-\xi_0(r_1k)\right)j_1(kR_2)\left(\left(\frac{1}{3}\mathbf{I}-\hat{\boldsymbol{u}}\hat{\boldsymbol{u}}^{\mathrm{T}}\right)J_0(ku)+\left(\hat{\boldsymbol{u}}\hat{\boldsymbol{u}}^{\mathrm{T}}-\hat{\boldsymbol{v}}\hat{\boldsymbol{v}}^{\mathrm{T}}\right)J_1(ku)\frac{1}{ku}\right).$$ (S43)

To proceed, we must consider the integrals in two separate cases: where spheres are either inside the intra-axonal space (i.e. $u + R_2 < r_1$, $R_2 < r_1$) or outside the cylinder in the extra-axonal space (i.e. $R_2 + R_1 < u$).

Sphere inside cylinder $u + R_2 < r_1$ and $R_2 < r_1$

When the sphere resides inside the cylinder layer, the two types of radial integrals in Eq. (S43) adds to zero (which follows from GR(6.573.2)), i.e.

$$\sqrt{\frac{\pi}{2R_2}} \int dk \frac{1}{k^{\frac{3}{2}}} J_0(ku) J_{\frac{3}{2}}(kR_2)\left(\xi_0(R_1 k) - \xi_0(r_1 k)\right) = 0, \tag{S44}$$

and

$$\int dk \frac{1}{k^{\frac{5}{2}}}\left(\xi_0(R_1 k) - \xi_0(r_1 k)\right) J_{\frac{3}{2}}(kR_2) J_1(ku) = 0. \tag{S45}$$

Hence no cross-contribution is associated with spheres inside the cylinder layers. This is sensible as this contribution can be seen as the induced frequency at a point (here a sphere) inside a cylindrical shell, which is known to be 0.

Spheres outside cylinder $R_2 + R_1 < u$

For the case where the sphere resides outside the cylinder, only one of the two unique integrals yields zero, i.e.

$$\int dk \frac{1}{k} J_0(ku) j_1(kR_2)\left(\xi_0(R_1 k) - \xi_0(r_1 k)\right) = 0. \tag{S46}$$

The first term in Eq. (S43), for a single layer and sphere is thus (cf. GR6.578.1)

$$\begin{aligned} \frac{3\zeta_2}{\zeta^{\mathrm{W}} R_2} \int dk \frac{1}{u k^{\frac{5}{2}}}\left(\xi_0(R_1 k) - \xi_0(r_1 k)\right) J_{\frac{3}{2}}(kR_2) J_1(ku)\left(\hat{\boldsymbol{u}}\hat{\boldsymbol{u}}^{\mathrm{T}} - \hat{\boldsymbol{v}}\hat{\boldsymbol{v}}^{\mathrm{T}}\right) \\ = \frac{1}{2}\frac{\zeta_2}{\zeta^{\mathrm{W}}} \frac{(R_1)^2 - (r_1)^2}{u^2}\left(\hat{\boldsymbol{u}}\hat{\boldsymbol{u}}^{\mathrm{T}} - \hat{\boldsymbol{v}}\hat{\boldsymbol{v}}^{\mathrm{T}}\right) \end{aligned},$$

If we rotate the cylinders an angle ϕ along $\hat{\boldsymbol{n}}$ (rotation axis), Eq. (S47) becomes

$$\frac{1}{2}\frac{\zeta_2}{\zeta^{\mathrm{W}}}\frac{\left(R_1\right)^2-\left(r_1\right)^2}{u^2}\left(\cos\left(2\phi\right)\left(\hat{\boldsymbol{u}}\hat{\boldsymbol{u}}^{\mathrm{T}}-\hat{\boldsymbol{v}}\hat{\boldsymbol{v}}^{\mathrm{T}}\right)+\sin\left(2\phi\right)\left(\hat{\boldsymbol{v}}\hat{\boldsymbol{u}}^{\mathrm{T}}+\hat{\boldsymbol{u}}\hat{\boldsymbol{v}}^{\mathrm{T}}\right)\right),\text{(cylinder target, sphere source)}.$$

$$\text{(S48)}$$

Due to the symmetry of $\Gamma\left(\boldsymbol{k}\right)$ for one layer and external sphere, Eq. (S48) corresponds to the well-known result for the local *microscopic* field outside a cylinder shell, as expected[4]. If we consider Eq. (S48) and sum over all external spheres for each spherical population and all spheres in both the cylinder bilayers and extra-axonal space assuming they are positioned axially symmetric to the layer, the contribution cancels out.

Looking at the last term of Eq. (S41), and summing over both multiple layers, cylinders and spheres, the only contribution left from the cross-correlation between field inducing spheres and reporting cylinders to the Lorentzian tensor $\mathbf{L}=-\chi\mathbf{N}$ from all spherical sources is

$$\mathbf{L}=\frac{\zeta^{\mathrm{C}}\left(\chi^{\mathrm{M}}\zeta^{\mathrm{M}}+\chi^{\mathrm{A}}\zeta^{\mathrm{A}}+\chi^{\mathrm{E}}\zeta^{\mathrm{E}}\right)}{\zeta^{\mathrm{W}}}\frac{1}{2}\left(\mathbf{T}-\frac{1}{3}\mathbf{I}\right),\text{(cylinder targets and sphere sources)}.\quad\text{(S49)}$$

Figure S4 shows a good agreement between Eq. (S49) to our simulation (see description in the beginning of supporting material) for each demagnetization tensor contribution between the cylinder as target and intra-axonal spheres (A), spheres in MW (M) or extra-axonal spheres (E) as sources, respectively.

Typically, $\zeta^{\mathrm{C}}/\zeta^{\mathrm{W}}\sim 0.5$ which means that this contribution can only be neglected if the spheres' bulk susceptibilities are sufficiently low.

Eigenvalues of $\mathbf{N}\zeta^{\mathrm{W}}/(\zeta^{\mathrm{S}}\zeta^{\mathrm{C}})$ (cylinder target, sphere sources)
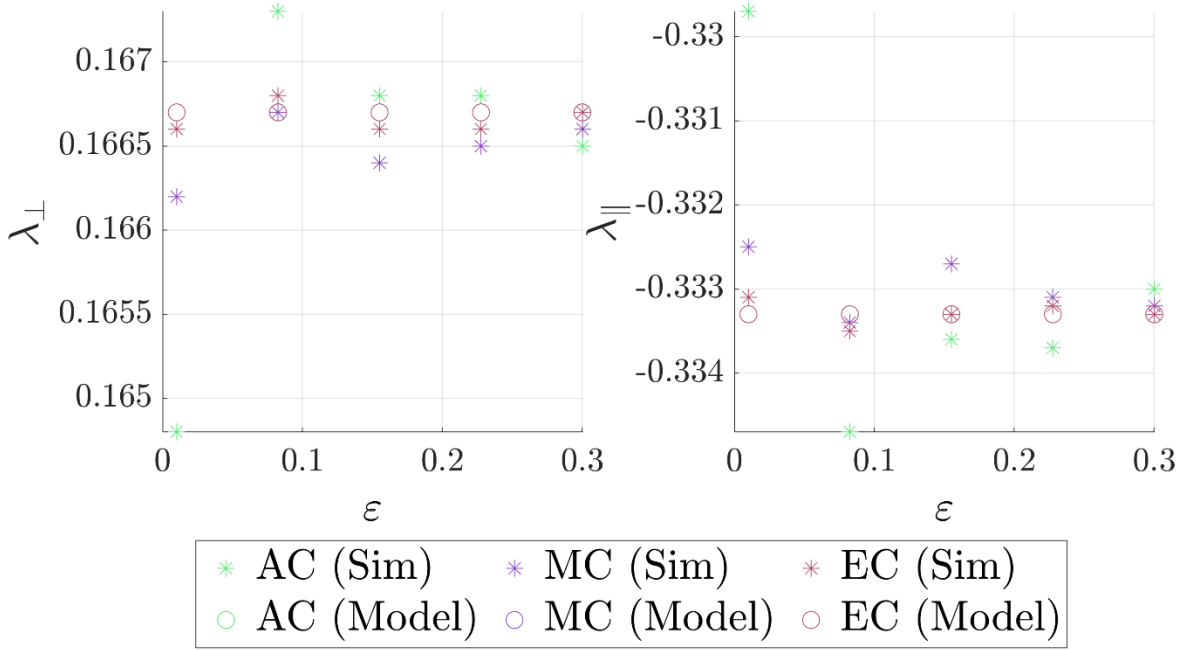

Figure S4 - Demagnetization tensor eigenvalues from cross-correlation between spheres and cylinders: Here from a population of spheres induced in the surrounding cylinder layers. The left figure shows the average perpendicular eigenvalue $\lambda_\perp$, and the right figure shows the parallel $\lambda_\parallel$, wrt. to the axes of the cylinder. The x-axis shows the density ε of spheres in a given water compartment.

Demagnetization tensor from cylindrical sources and spherical targets

We now consider the cross-contribution to the frequency shift inside a reporting sphere of radius R_1 and volume fraction ζ_1 placed at the origin generated by a single cylinder layer with radii r_2, R_2 and volume fraction ζ_2 positioned at $\boldsymbol{u}$. Its contribution is described by the tensor-valued cross-correlation function $\boldsymbol{\Gamma}(\boldsymbol{k})$ and is given by Eqs. (S14) and (S28)

$$\boldsymbol{\Gamma}(\boldsymbol{k}) = 12\pi^2 \delta(\boldsymbol{k}\cdot\hat{\boldsymbol{n}}) e^{i\boldsymbol{k}\cdot\boldsymbol{u}} \zeta_1 \frac{j_1(kR_1)}{kR_1}\left\{ \boldsymbol{\chi}_0 \left(\xi_0(kR_2) - \xi_0(kr_2) \right) \right.$$

$$\left. - \operatorname{Re}\left\{ \boldsymbol{\chi}_2 e^{2i\psi} \right\} \left(\xi_2(kR_2) - \xi_2(kr_2) \right) \right\}, \text{ (sphere target and cylinder source).}$$

$$- 4\pi^2 \zeta_2 \zeta_1 \boldsymbol{\chi}_0 \frac{\delta(k)\delta(\boldsymbol{k}\cdot\hat{\boldsymbol{n}})}{k}$$

$$\text{(S50)}$$

17

The first and third term in Eq. (S50) is equivalent to the previously considered cross-contribution between cylinders as the target and spheres the sources (cf. Eq. (S40)). Here we found that only the third contributes to the Lorentzian tensor $\mathbf{L}$ after summing over cylinders and spheres. This means we need only to consider the second and third terms. We start by considering the contribution to the Lorentzian tensor from the second ψ-dependent term of $\mathbf{\Gamma}(\boldsymbol{k})$

$$\frac{3}{\pi R_1}\frac{\zeta_1}{\zeta^{\mathrm{W}}}\int dk\int d\hat{\boldsymbol{k}}\,\Upsilon(\boldsymbol{k})\delta(\boldsymbol{k}\cdot\hat{\boldsymbol{n}})e^{i\boldsymbol{k}\cdot\boldsymbol{u}}\operatorname{Re}\left\{\chi_2 e^{2i\psi}\right\}\left(\xi_2(kR_2)-\xi_2(kr_2)\right)j_1(kR_1). \tag{S51}$$

The angular integral of Eq. (S51) is

$$\begin{aligned}&\frac{1}{\pi}\int d\hat{\boldsymbol{k}}\,\Upsilon(\boldsymbol{k})\delta(\boldsymbol{k}\cdot\hat{\boldsymbol{n}})e^{i\boldsymbol{k}\cdot\boldsymbol{u}}\operatorname{Re}\left\{\chi_2 e^{2i\psi}\right\}\\&=\frac{\Delta\chi}{2}\left(\left(\hat{\boldsymbol{n}}\hat{\boldsymbol{n}}^{\mathrm{T}}-\mathbf{I}\right)J_0(ku)-\frac{1}{6}\left(\hat{\boldsymbol{u}}\hat{\boldsymbol{u}}^{\mathrm{T}}-\hat{\boldsymbol{v}}\hat{\boldsymbol{v}}^{\mathrm{T}}\right)J_2(ku)\right)\end{aligned} \tag{S52}$$

Plugging Eq. (S52) into Eq. (S51) yields the angular integral (excluding some front factors)

$$\int dk\left(\left(\hat{\boldsymbol{n}}\hat{\boldsymbol{n}}^{\mathrm{T}}-\mathbf{I}\right)J_0(ku)-\frac{1}{6}\left(\hat{\boldsymbol{u}}\hat{\boldsymbol{u}}^{\mathrm{T}}-\hat{\boldsymbol{v}}\hat{\boldsymbol{v}}^{\mathrm{T}}\right)J_2(ku)\right)\left(\xi_2(kR_2)-\xi_2(kr_2)\right)j_1(kR_1). \tag{S53}$$

Again, Eq. (86) has to be considered separately, for a sphere inside or outside the cylinder.

Sphere outside cylinder $R_1+R_2<u$

The first radial integral including $J_0(ku)$ in Eq. (S53) is zero which follows from GR(6.573.1), and the independence of $J_0(kr_2)$ and $J_0(kR_2)$ in the integrand for such combinations of Bessel functions and powers[8,9]

$$\int dk J_0(ku)\left(\xi_2(kR_2)-\xi_2(kr_2)\right)j_1(kR_1)=0, \tag{S54}$$

The last integral in Eq. (S53) relating to $J_2(ku)$ also integrates to zero, which follows from GR(6.573.2) and GR(9.180.4)

$$\frac{1}{R_1}\frac{\zeta_1}{\zeta^{\mathrm{W}}}\frac{1}{2}\int dk J_2(k\Delta u)\left(\xi_2(kR_2)-\xi_2(kr_2)\right)j_1(kR_1)=0. \tag{S55}$$

Hence, Eq. (S53) is zero.

Sphere inside cylinder $u + R_1 < r_2$ and $R_1 < r_2$

The last to consider is contributions from spheres residing within the cylinder (i.e. $u + R_1 < r_2$, $R_1 < r_2$). The only non-zero radial integral of Eq. (S53) comes from $J_0(ku)$ (which follows from GR(6.573.1)), which is independent of $J_0(ku)$ [8,9]. Using GR(6.577.2), Eq. (S53) becomes

$$\sqrt{\frac{\pi}{2R_1}} \int dk \, \frac{J_{\frac{3}{2}}(kR_1)}{\sqrt{k}} J_0(ku) \left(\xi_2(kR_2) - \xi_2(kr_2) \right) = -\frac{1}{3} R_1 \ln \frac{r_2}{R_2}. \tag{S56}$$

Here we only considered a cylinder made up of a single layer. This means that we first have to sum over spheres inside a single cylinder, either being in the intra-axonal space or in the MW bilayers.

Summing over all intra-axonal spheres and cylinder layers constituting the multi-layered cylinder of the single cylinder we can define a new lambda parameter λ_1^A

$$\lambda_1^A = \zeta_1^A \frac{6}{\zeta^W \zeta_2} \sum_q \ln\left(\frac{r_q}{R_q}\right), \quad \text{(intra-axonal spheres)}, \tag{S57}$$

which acts as a correction to the previously derived λ_1 parameter, Equation (S21), for the cylinders. Here ζ_1^A is understood as the total volume of spheres in the intra-axonal space of a single cylinder. A similar correction arise from spheres within the MW bilayers, where we use ζ_q^M to indicate the total volume fraction of the spheres inside the q'th MW layer

$$\lambda_1^M = \frac{6}{\zeta^W \zeta_2} \sum_{q'>q} \zeta_q^M \ln\left(\frac{r_{q'}}{R_{q'}}\right), \quad \text{(myelin water spheres)}. \tag{S58}$$

Left to do is summing over N cylinders in Eqs. (S57) and (S58). For this we define a combined parameter $\lambda^S \equiv \lambda^A + \lambda^M = N\left(\langle \lambda_1^A \rangle + \langle \lambda_1^M \rangle \right)$. Since $\lambda^A + \lambda^M$ has an opposite sign of λ^C, the presence of spherical inclusions within the intra-axonal space and MW bilayers effectively reduce the Larmor frequency shift caused by susceptibility anisotropy $\Delta\chi$. This makes sense as it reduces the water fraction reporting the Larmor frequency shift from within that compartment.

Using Eqs. (S49), (S53) and λ^{S}, we obtain for the Lorentzian tensor from cylindrical sources and spherical targets

$$\mathbf{L} = -\lambda^{\mathrm{S}}\frac{\Delta\bar{\chi}}{12}(\mathbf{T}-\mathbf{I}) + \frac{\zeta^{\mathrm{S}}}{\zeta^{\mathrm{W}}}\left(\bar{\chi}^{\mathrm{C}}\frac{1}{2}\left(\mathbf{T}-\frac{1}{3}\mathbf{I}\right) - \frac{\Delta\bar{\chi}}{12}\left(\mathbf{T}+\frac{1}{3}\mathbf{I}\right)\right),\qquad (\mathrm{S}59)$$

(Cylinder sources, sphere targets).

Figure S5 shows a good agreement between Eq. (S59) to our simulation (see description in the beginning of the supporting material) for each Lorentzian tensor contribution between the cylinder source and intra-axonal spheres (A), spheres in MW (M) or extra-axonal spheres (E) as target, respectively.

Eigenvalues of $\mathbf{L}\zeta^{\mathrm{W}}/(\zeta^{\mathrm{S}}\zeta^{\mathrm{C}})$, (cylinder source, sphere targets)

* A (Sim)   * M (Sim)   * E (Sim)
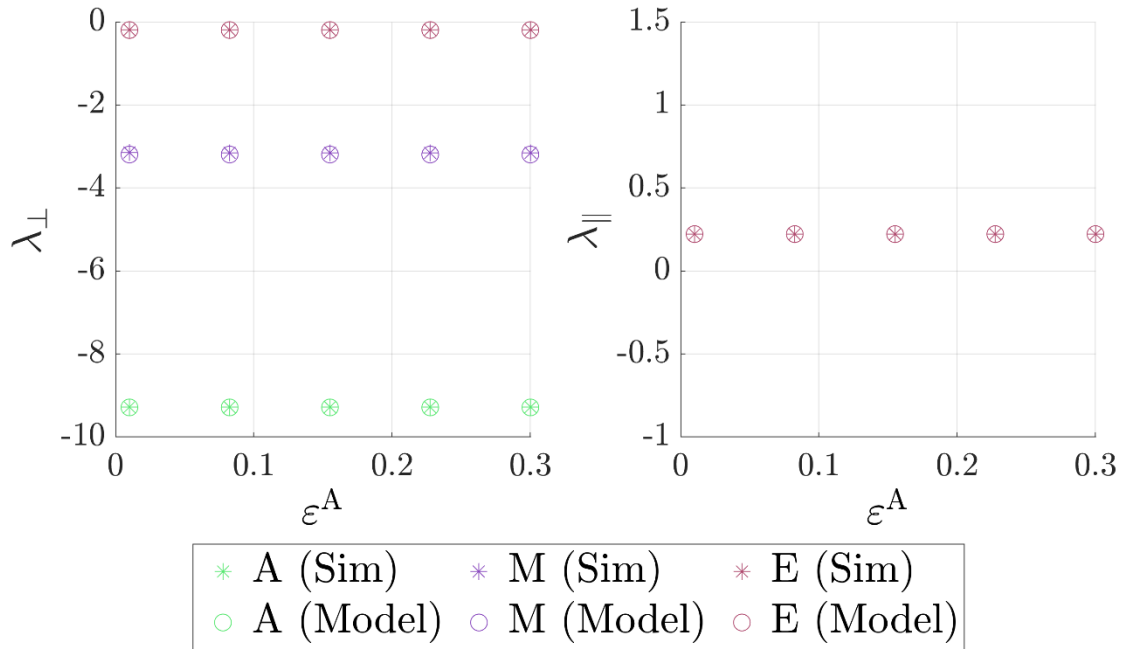∘ A (Model) ∘ M (Model) ∘ E (Model)

Figure S5 - Lorentzian tensor eigenvalues from cross-correlation between cylinders and spheres: Here from cylinders with susceptibility set to unity $\Delta\chi = \chi^{\mathrm{C}} = 1$, induced in a population of spheres. The ground truth signal was made from simulations, where every cylinder layer was associated a magnetic susceptibility tensor, which was computed using $\chi^{\mathrm{C}}(\phi)$, cf. Eq. (S6). The left figure shows the average perpendicular eigenvalue $\lambda_{\perp}$, and the right figure shows the parallel $\lambda_{\parallel}$, wrt. to the axes of the cylinder. The x-axis shows the density ε of spheres in a given water compartment.

S4) Lorentzian tensor from relaxed myelin water

Last to consider is the cross-contribution to the frequency shift when MW is fully relaxed. If MW is not relaxed, then $\zeta^W = 1 - \zeta$, i.e. equal to the negated volume fraction of the whole magnetized structure. In that case, no additional frequency contributions must be considered. However, when MW is fully relaxed, then $\zeta^W = 1 - \zeta - \zeta^{MW}$, where ζ^{MW} is the volume fraction of all the water in the MW compartment. In addition, this gives rise to two additional Lorentzian tensors which must be subtracted from our earlier results, since they include the frequency shift in MW: The first describes the frequency shift induced inside MW from cylinders with magnetic susceptibility χ^C, and the second describes the frequency shift induced inside MW from all spheres with total magnetic susceptibility χ^S. Its contribution to the mesoscopic frequency shift is however easy to deduce, at it is basically the same frequency contribution as for the spheres in MW – the only difference is, that upon coarse-graining this MW compartment, the density now relates to the water content ζ^{MW} and not sphere content ζ^M. In total we get the Lorentzian tensor from MW

$$
\begin{aligned}
\mathbf{L} = &-\lambda^{MW} \frac{\Delta\bar{\chi}}{12}(\mathbf{T}-\mathbf{I}) + \frac{\zeta^{MW}}{\zeta^W}\left(\bar{\chi}^C \frac{1}{2}\left(\mathbf{T}-\frac{1}{3}\mathbf{I}\right) - \frac{\Delta\bar{\chi}}{12}\left(\mathbf{T}+\frac{1}{3}\mathbf{I}\right)\right) \\
&-\frac{\bar{\chi}^M}{\zeta^W}\left(1-\zeta^{MW}-\zeta^M-\zeta^A-\zeta^E-\zeta^C\right)\frac{1}{2}\left(\mathbf{T}-\frac{1}{3}\mathbf{I}\right) + \frac{\zeta^{MW}\left(\bar{\chi}^A+\bar{\chi}^E\right)}{\zeta^W}\frac{1}{2}\left(\mathbf{T}-\frac{1}{3}\mathbf{I}\right).
\end{aligned}
\tag{S60}
$$

where

$$
\lambda^{MW} = \mathrm{N}\left\langle \lambda_1^{MW}\right\rangle, \quad \lambda_1^{MW} = \frac{6}{\zeta^W \zeta_2}\sum_{q'>q}\left(\zeta_{R_q}^C - \zeta_{r_q}^C - \zeta_q^M\right)\ln\left(\frac{R_{q'}}{r_{q'}}\right).
\tag{S61}
$$

The single cylinder parameter λ_1^{MW} describes the correction for all myelin water within a single cylinder of volume fraction ζ_2.

S5) Total Mesoscopic frequency shift $\bar{\Omega}^{Meso}$

Combining all contributions to the total mesoscopic frequency shift within our model picture of spherical and cylindrical inclusions, we get the total frequency shift associated with magnetic microstructure within the mesoscopic sphere

$$
\bar{\Omega}^{Meso} = \gamma \mathrm{B}_0 \hat{\mathbf{B}}^T \mathbf{L} \hat{\mathbf{B}},
\tag{S62}
$$

where

$$\mathbf{L} = -\left(\bar{\chi}^{C} + \bar{\chi}^{M}\right)\frac{1}{2}\left(\mathbf{T} - \frac{1}{3}\right) + \gamma \mathbf{B}_0 \frac{\Delta\bar{\chi}}{12}\left(\mathbf{T}(1-\lambda) + \left(\lambda + \frac{1}{3}\right)\right)$$

$$+ \gamma \mathbf{B}_0 \bar{\chi}^{A} \frac{\left(\zeta^{MW} + \zeta^{C} - \zeta^{A}\frac{\left(1-\tilde{\zeta}^{A}\right)}{\tilde{\zeta}^{A}} + \zeta^{E}\right)}{\zeta^{W}}\frac{1}{2}\left(\mathbf{T} - \frac{1}{3}\right) \qquad (S63)$$

$$+ \gamma \mathbf{B}_0 \bar{\chi}^{E} \frac{\left(\zeta^{MW} + \zeta^{C} + \zeta^{A} - \zeta^{E}\frac{\tilde{\zeta}^{C}}{1-\tilde{\zeta}^{C}}\right)}{\zeta^{W}}\frac{1}{2}\left(\mathbf{T} - \frac{1}{3}\right)$$

When MW is fully relaxed, we get the following effective lambda parameter

$$\lambda = \mathrm{N}\langle\lambda_1\rangle = \mathrm{N}\left(\langle\lambda_1^C\rangle + \langle\lambda_1^A\rangle + \langle\lambda_1^M\rangle + \langle\lambda_1^{MW}\rangle\right) \qquad (S64)$$

where

$$\lambda_1 = -\zeta_1^{AW}\frac{6}{\zeta^{W}\zeta_1}\sum_q \ln\left(\frac{r_q}{R_q}\right). \qquad (S65)$$

The volume fraction ζ_1^{AW} denotes the intra-axonal water fraction inside a single cylinder of volume fraction ζ_1. The largest contribution from the magnetic susceptibilities $\bar{\chi}^{E}$ and $\bar{\chi}^{A}$ scale as $\zeta^{C} / \zeta^{W} \sim 0.5$, but if the susceptibilities are small, then we may neglect the last two terms of Eq. (S63). When MW is fully relaxed, $\bar{\chi}^{MW}$ contributes to $\bar{\Omega}^{Meso}$ in an equal footing as $\bar{\chi}^{C}$.
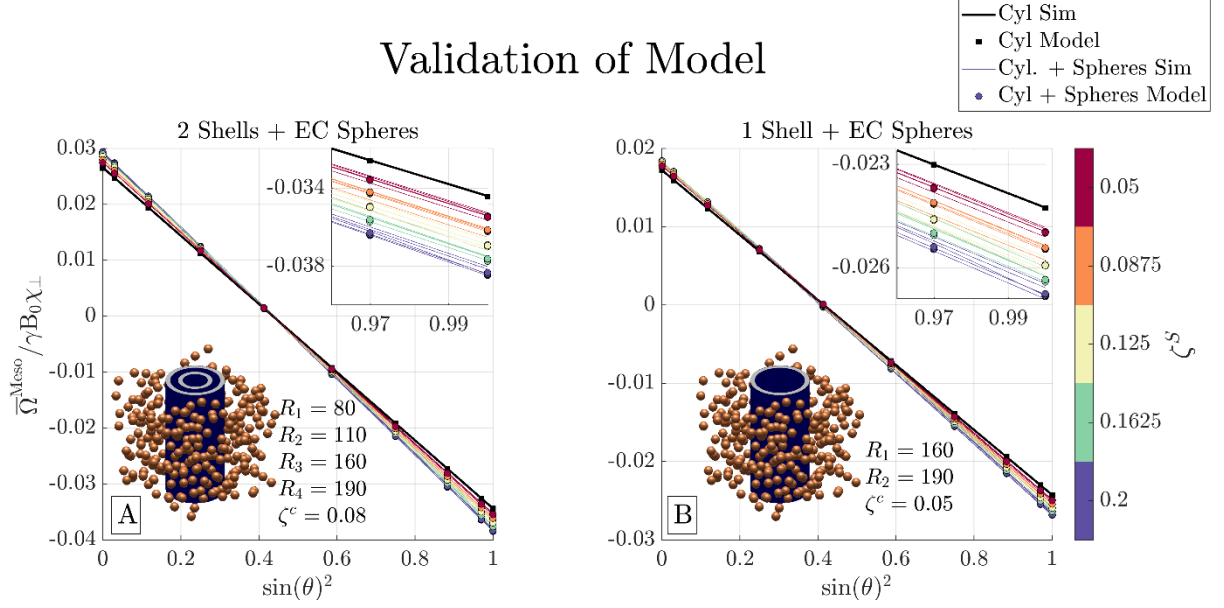
Figure S6 – Mesoscopic frequency shift $\overline{\Omega}^{\text{Meso}}$ from a multilayer cylinder and external spheres: A shows $\overline{\Omega}^{\text{Meso}}$ from a 2-layer cylinder with radii and volume fraction shown above. The frequency shift was simulated on 800^3 grid units. The black line shows $\overline{\Omega}^{\text{Meso}}$ without spheres, and the colored lines indicate different volume fractions ζ^{C} of external spheres. The different lines for each color represent different radii of the spheres. **B** shows the same as **A**, but for a single layer cylinder.

Since our result for Eq. (S63) does consider any effects associated with a finite sphere radii, as the distribution of spheres in every water compartment was coarse grained (see A2), we include here an additional validation of Eq. (S63) for different sphere radii. Figure 15 shows $\overline{\Omega}^{\text{Meso}} / \gamma B_0 \overline{\chi}^{\text{C}}$ where $\overline{\chi}^{\text{C}} = \Delta \overline{\chi} = -\overline{\chi}^{\text{S}} < 0$ for a single cylinder of one and two layers, with radii R_i and volume fraction ζ^{C} described in Figure S6. The frequency shift was simulated on a grid of dimensions 800^3, similar to the supporting simulation . The volume fraction ζ^{S} of spheres external to the cylinder was varied from 0.01 to 0.2 which is indicated by different colored lines. The black line indicates no spheres. For each volume fraction ζ^{S}, the sphere radii were varied from 8 to 40 grid units and can be seen as the multiple lines for each color. We find that our model agrees with the simulations, not only for $\overline{\Omega}^{\text{Meso}} / \gamma B_0 \overline{\chi}^{\text{C}}$ from the cylinder alone (black line), but also the overall effect from the spheres. A small variation can be seen for each color from varying the radii, but this uncaptured dependence on sphere radius is small compared to the overall magnitude of $\overline{\Omega}^{\text{Meso}} / \gamma B_0 \overline{\chi}^{\text{C}}$.

S6) Macroscopic contribution $\overline{\Omega}^{\text{Macro}}(\mathbf{R})$

Last to consider is the macroscopic contribution from nearby voxels in the limit of a slowly varying magnetic microstructure on the macroscale. We previously found[2] this to be

$$\overline{\Omega}^{\text{Macro}}(\mathbf{R}) = \gamma B_0 \hat{\mathbf{B}}^{\text{T}} \sum_{\mathbf{R}'} \overline{\mathbf{Y}}(\mathbf{R} - \mathbf{R}') \overline{\chi}(\mathbf{R}') \hat{\mathbf{B}}. \tag{S66}$$

Using Eq. (S15) for the coarse-grained magnetic susceptibility of a cylinder and summing over them all including the bulk susceptibility across all spheres we get

$$\overline{\Omega}^{\text{Macro}}(\mathbf{R}) = \gamma B_0 \hat{\mathbf{B}}^{\text{T}} \sum_{\mathbf{R}'} \overline{\mathbf{Y}}(\mathbf{R} - \mathbf{R}') \left[\left(\overline{\chi}^{\text{C}}(\mathbf{R}') + \overline{\chi}^{\text{S}}(\mathbf{R}') \right) \mathbf{I} - \frac{\Delta\overline{\chi}(\mathbf{R}')}{2} \left(\mathbf{T}(\mathbf{R}') - \frac{1}{3} \mathbf{I} \right) \right] \hat{\mathbf{B}}. \tag{S67}$$

S7) Integrals and identities

Here we list all the non-trivial integrals and identities used from the table by Gradshteyn and Ryzhik [1], seventh edition. Equation numbers corresponds to the table numbers in their book. Identities have also been validated numerically.

$$\int_0^1 dx\, x J_\nu(\alpha x) J_\nu(\beta x) = \frac{\beta J_{\nu-1}(\beta x) J_\nu(\alpha x) - \alpha J_{\nu/1}(\alpha x) J_\nu(\beta x)}{\alpha^2 - \beta^2}, \ [\alpha \neq \beta, \nu > -1], \ \text{GR}(5.521.1)$$

$$\int_0^a dx\, J_1(x) = 1 - J_0(a), \ \text{GR}(6.511.7)$$

$$x J_{\nu-1}(x) + x J_{\nu+1}(x) = 2x J_\nu(x), \ \text{GR}(8.471.1)$$

$$\int_0^\infty dx\, \frac{1}{x^2} \left(1 - J_0(ax) \right) J_1(bx) = \begin{cases} -\dfrac{b}{4} \left(1 + 2\ln\left(\dfrac{a}{b} \right) \right), & [0 < b < a] \\[4mm] -\dfrac{a^2}{4b}, & [0 < a < b] \end{cases}, \ \text{GR}(6.533.3)$$

$$\int_0^{2\pi} d\phi \cos\big(k\cos(\phi)\big)\cos(n\phi) = 2\pi \cos\left(\frac{n\pi}{2}\right) J_n(k), \quad \text{GR(3.716.18)}$$

$$\int_0^\infty dx\, x^{\nu-M+1} J_\nu(bx) \prod_{i=1}^k J_{\mu_i}(a_i x) = 0, \quad M = \sum_{i=1}^k \mu_i,$$

$$\left[a_i > 0,\ \sum_{i=1}^k a_i < b < \infty,\ -1 < \operatorname{Re}\nu < \operatorname{Re}M + \frac{1}{2}k - \frac{1}{2} \right], \quad \text{GR(6.573.1)}$$

$$\int_0^\infty dx\, x^{\nu-M-1} J_\nu(bx) \prod_{i=1}^k J_{\mu_i}(a_i x) = 2^{\nu-M-1} b^{-\nu}\, \Gamma(\nu) \prod_{i=1}^k \frac{a_i^{\mu_i}}{\Gamma(\mu_i+1)}, \quad M = \sum_{i=1}^k \mu_i,$$

$$\left[a_i > 0,\ \sum_{i=1}^k a_i < b < \infty,\ 0 < \operatorname{Re}\nu < \operatorname{Re}M + \frac{1}{2}k + \frac{3}{2} \right], \quad \text{GR (6.573.2)}$$

$$\int_0^\infty dx\, x^{\rho-1} J_\lambda(ax) J_\mu(bx) J_\nu(cx) = 2^{\rho-1} a^\lambda b^\mu c^{-\lambda-\mu-\rho}\, \Gamma\left(\frac{\lambda+\mu+\nu+\rho}{2}\right) \frac{1}{\Gamma(1+\lambda)\Gamma(1+\mu)\Gamma\left(1-\frac{\lambda+\mu-\nu+\rho}{2}\right)} \cdot$$

$$F_4\left(\frac{\lambda+\mu-\nu+\rho}{2}, \frac{\lambda+\mu+\nu+\rho}{2}; 1+\lambda, 1+\mu; \frac{a^2}{c^2}, \frac{b^2}{c^2}\right).$$

$$\big[a > 0,\ b > 0,\ 0 < a+b < c,\ \operatorname{Re}\{\lambda+\mu+\nu+\rho\} > 0,\ \operatorname{Re}\rho < 5/2 \big], \qquad \text{GR(6.578.1)}$$

where F_4 is the Appell hypergeometric series of two variables

$$F_4(\alpha,\beta;\gamma,\gamma';x,y) = \sum_{m=0}^\infty \sum_{n=0}^\infty \frac{(\alpha)_{m+n}(\beta)_{m+n}}{(\gamma)_m (\gamma')_n\, m!n!} x^m y^n, \quad \text{GR (9.180.4)}$$

$$(\alpha)_m = \prod_{k=0}^{m-1}(\alpha+k),$$

and $(\alpha)_m$ is the Pochhammer symbol.

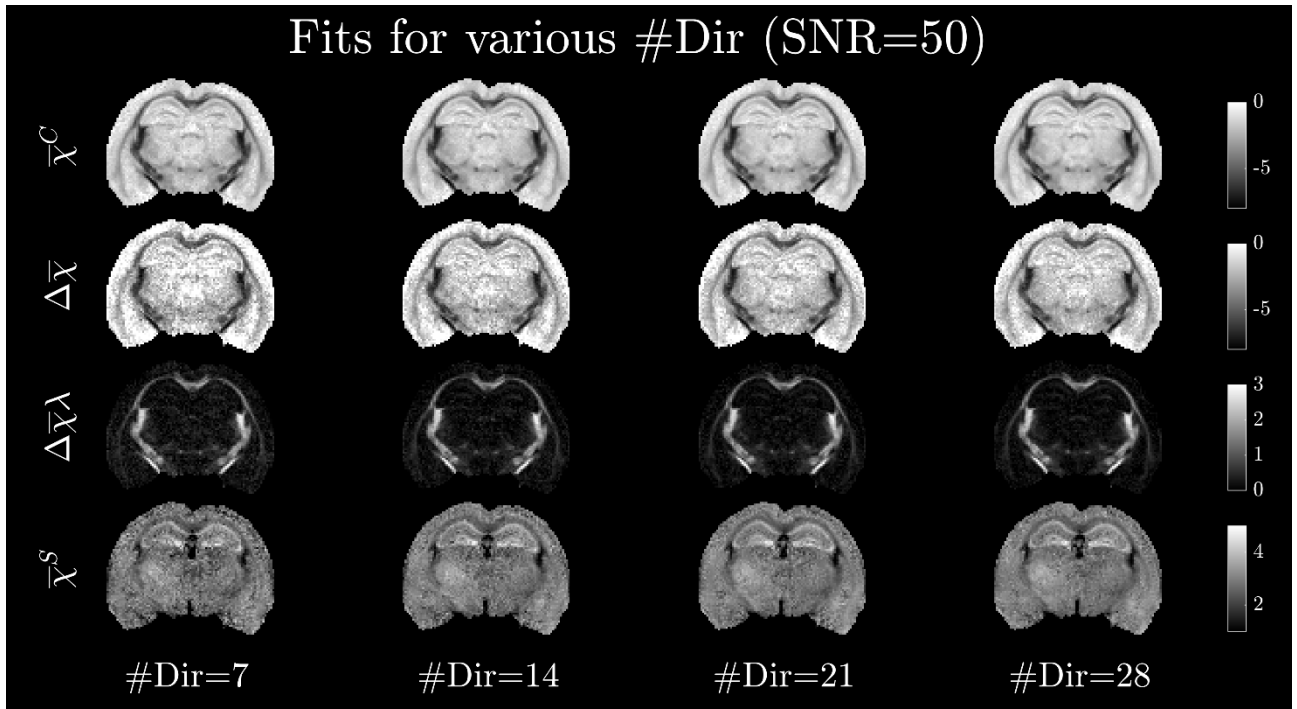## S8) Supplementary figures for simulation b)

Figure S7 – Simulation (b): Susceptibility fitting maps. Fitting maps for various numbers of sample orientations and a fixed SNR=50 and maximum tilt angle of 90 degrees.
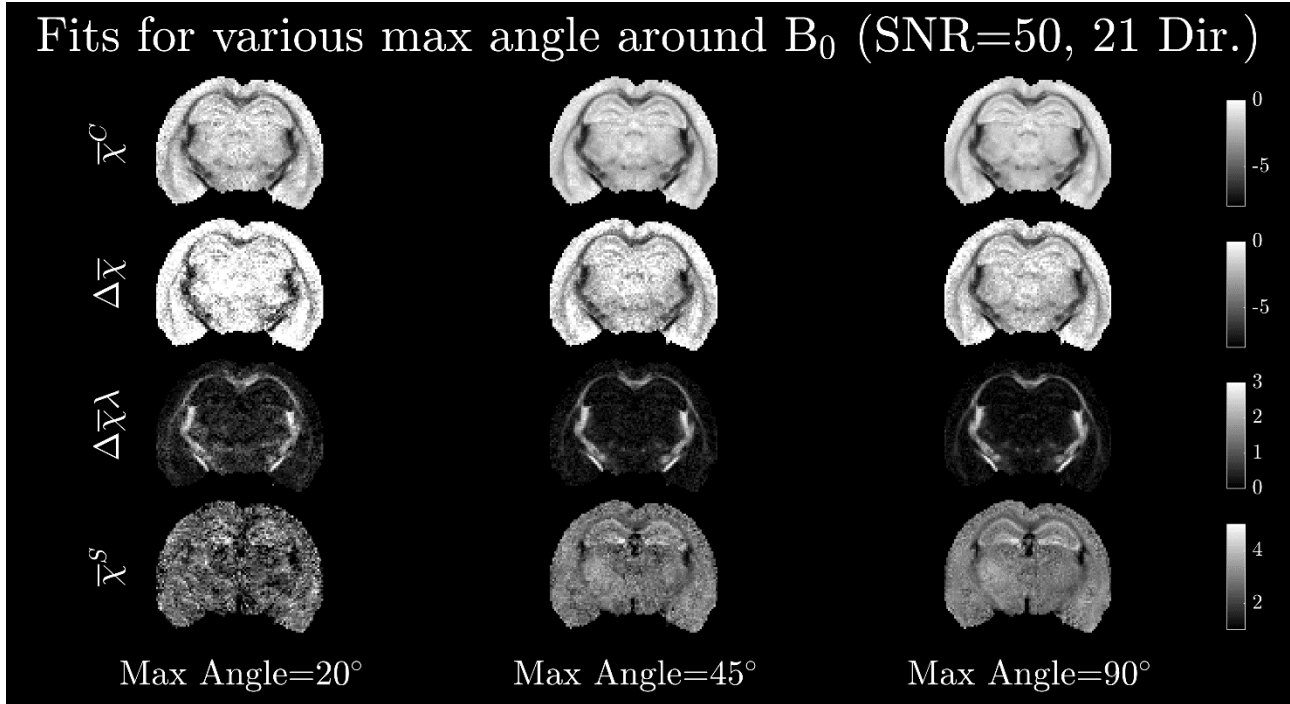
Figure S8 – Simulation (b): Susceptibility fitting maps. Fitting maps for various maximum tilt angles and a fixed SNR=50 and 21 sample orientations.

References

1. Zwillinger D. *Table of Integrals, Series, and Products: Eighth Edition*. Elsevier Inc.; 2014. doi:10.1016/C2010-0-64839-5

2. Sandgaard AD, Shemesh N, Kiselev VG, Jespersen SN. Larmor frequency shift from magnetized cylinders with arbitrary orientation distribution. *NMR Biomed*. 2023;36(3):e4859. doi:10.1002/nbm.4859

3. Sandgaard AD, Kiselev VG, Henriques RN, Shemesh N, Jespersen SN. Incorporating the effect of white matter microstructure in the estimation of magnetic susceptibility in ex vivo mouse brain. *Magn Reson Med*. September 2023. doi:10.1002/MRM.29867

4. Wharton S, Bowtell R. Fiber orientation-dependent white matter contrast in gradient echo MRI. *Proc Natl Acad Sci U S A*. 2012;109(45):18559-18564. doi:10.1073/pnas.1211075109

5. Sukstanskii AL, Yablonskiy DA. On the role of neuronal magnetic susceptibility and structure symmetry on gradient echo MR signal formation. *Magn Reson Med*. 2014;71(1):345-353. doi:10.1002/mrm.24629

6. Arfken GB, Weber HJ, Spector D. Mathematical Methods for Physicists, 4th ed. *Math Methods Phys Eng Am J Phys*. 1999;67:958. doi:10.1119/1.19217

7. Thorne KS. Multipole expansions of gravitational radiation. *Rev Mod Phys*. 1980;52(2):299-339. doi:10.1103/RevModPhys.52.299

8. Watson GN (George N. A treatise on the theory of Bessel functions. 1995:804.

9.   Bailey WN. Some Infinite Integrals Involving Bessel Functions. *Proc London Math Soc*. 1936;s2-40(1):37-48. doi:10.1112/PLMS/S2-40.1.37